HHS Public Access

Author manuscript

Clin Cancer Res. Author manuscript; available in PMC 2020 September 15.

Published in final edited form as:

Clin Cancer Res. 2020 March 15; 26(6): 1420–1431. doi:10.1158/1078-0432.CCR-19-2625.

Inhibition of MDSC trafficking with SX-682, a CXCR1/2 inhibitor, enhances NK cell immunotherapy in head and neck cancer models

Sarah Greene[1,2], **Yvette Robbins**[1], **Wojciech Mydlarz**[3], **Angel Huynh**[1], **Nicole Schmitt**[3], **Jay Friedman**[1], **Lucas A. Horn**[4], **Claudia Palena**[4], **Jeffrey Schlom**[4], **Dean Y. Maeda**[5], **John A. Zebala**[5], **Paul E. Clavijo**[1], **Clint T. Allen**[1,3]

[1]Translational Tumor Immunology Program, National Institute on Deafness and Other Communication Disorders, Bethesda, MD

[2]National Institutes of Health Medical Research Scholars Program

[3]Department of Otolaryngology-Head and Neck Surgery, Johns Hopkins School of Medicine, Baltimore, MD

[4]Laboratory of Tumor Immunology and Biology, National Cancer Institute, Bethesda, MD

[5]Syntrix Pharmaceuticals, Auburn, WA

Abstract

Purpose—Natural killer (NK) cell-based immunotherapy may overcome obstacles to effective T cell-based immunotherapy such as the presence of genomic alterations in interferon response genes and antigen presentation machinery. All immunotherapy approaches may be abrogated by the presence of an immunosuppressive tumor microenvironment present in many solid tumor types, including head and neck squamous cell carcinoma (HNSCC). Here, we studied the role of myeloid derived suppressor cells (MDSC) in suppressing NK cell function in HNSCC.

Experimental Design—The ability of peripheral and tumor infiltrating MDSC from mice bearing murine oral cancer 2 (MOC2) non-T cell inflamed tumors and from HNSCC patients to suppress NK cell function was studied with real-time impedance and ELISpot assays. The therapeutic efficacy of SX-682, a small molecule inhibitor of CXCR1 and CXCR2, was assessed in combination with adoptively transferred NK cells.

Results—Mice bearing MOC2 tumors pathologically accumulate peripheral CXCR2+ neutrophilic-MDSC (PMN-MDSC) that traffic into tumors and suppress NK cell function through TGF-β and production of H_2O_2. Inhibition of MDSC trafficking with orally bioavailable SX-682 significantly abrogated tumor MDSC accumulation and enhanced the tumor infiltration, activation and therapeutic efficacy of adoptively transferred murine NK cells. Patients with HNSCC harbor significant levels of circulating and tumor infiltrating CXCR1/2+ CD15+ PMN-MDSC and

Corresponding author: Clint Allen, MD, 10 Center Drive, Room 7N240C, Bethesda, MD 20817, Phone: 301-827-5620; clint.allen@nih.gov.

Conflicts of interest: JZ and DM are employees of Syntrix Pharmaceuticals. Otherwise the authors declare no potential conflicts of interest.

CD14+ monocytic-MDSC. Tumor MDSC exhibited greater immunosuppression than those in circulation. HNSCC tumor MDSC immunosuppression was mediated by multiple, independent, cell-specific mechanisms including TGF-β and nitric oxide.

Conclusions—The clinical study of CXCR1/2 inhibitors in combination with adoptively transferred NK cells is warranted.

Keywords

Myeloid derived suppressor cell; chemotaxis; NK cellular therapy; functional analysis; head and neck squamous cell carcinoma

Introduction

Subclones of tumor cells within heterogeneous carcinomas harbor genomic alterations that confer resistance to T cell anti-tumor immunity. Altered genes encoding components of the interferon response pathway(1), antigen processing(1,2), and antigen presentation(1–3) have been identified in tumors from patients that have failed T cell-based immunotherapy. Such clonal cell populations may be irreversibly insensitive to detection or elimination by T cells, but may retain the ability to be detected by natural killer (NK) cells through antigen- and MHC-independent mechanisms. Engineered NK cellular therapies are under clinical investigation (NCT03027128, NCT03387111).

Carcinomas such as head and neck squamous cell carcinoma (HNSCC) develop an immunosuppressive microenvironment through multiple mechanisms(4). Myeloid derived suppressor cells (MDSC), a heterogeneous population of immunosuppressive myeloid cells, are pathologically expanded in mice and humans with cancer and are recruited into tumors through chemokine gradients(5–8). Both neutrophilic and monocytic subsets of MDSC suppress T cell function primarily through production of arginase(7,8). The effects that MDSC may have on endogenous NK cells or NK cell-based immunotherapies are less understood.

Here, we demonstrated in an immunologically “cold” syngeneic model of oral cancer (mouse oral cancer 2, or MOC2) that Ly6G^{hi} neutrophilic-MDSC (PMN-MDSC) suppress NK function through multiple independent mechanisms. Inhibition of CXCR2+ PMN-MDSC trafficking into MOC2 tumors with SX-682, a small molecule dual inhibitor of CXCR1/2, enhanced tumor infiltration, activation, and the therapeutic efficacy of adoptively transferred NK cells. The mechanism of this enhancement was due to inhibition of PMN-MDSC trafficking and independent of direct anti-tumor effects. Additionally, we verified the accumulation of CD15+CD14- PMN-MDSC and CD15-CD14+HLA-DR^{low} monocytic-MDSC (M-MDSC) positive for both CXCR1 and CXCR2 in the circulation of patients with advanced HNSCC. PMN-MDSC and M-MDSC that trafficked into HNSCC tumors demonstrated enhanced suppressive capacity of healthy donor NK cells compared to circulating MDSC through multiple, independent mechanisms. Together, data from this study establish the role of MDSC in abrogating NK cell function in mice and humans, and provide the rationale for the clinical study of CXCR1/2 inhibitors in combination with adoptively transferred NK cells.

Methods

Cell culture, animal studies and human specimens

MOC2 cells were cultured as described(9). Genomically characterized cell stocks were used at low passage number (<30) for all experiments, verified free of mycoplasma and murine associated pathogens and authenticated with CD44 and MHC expression. KIL murine NK cells were purchased from Kerafast and cultured as described(10). Four days prior to use, low passage number KIL (<10) were exposed to murine IL-2 (20 ng/mL). In some experiments, GM-CSF (10 ng/mL) was added to media for MDSC culture(11). SX-682 was obtained under a Cooperative Research and Development Agreement with Syntrix Pharmaceuticals. Tumors were established by subcutaneous injection of MOC2 cells (1×10^5 cells in PBS) in the flanks of wild-type C57BL/6 mice (Taconic). Tumor volumes were obtained three times weekly and calculated as (length x width^2)/2. Control high fat chow and chow formulated with SX-682 (drug added to expose mice to 500 mg/kg body weight/day) was obtained from Research Diets, Inc. KIL were adoptively transferred via intraperitoneal injection. All human peripheral blood and HNSCC tumor biopsies were obtained under an IRB-approved biospecimen procurement protocol (NIH protocol number 18-DC-0051) conducted in accordance with the U.S. Common Rule after obtaining informed written consent.

Flow cytometry of murine and human samples

For details of flow cytometry, see Supplemental Methods.

Trafficking of adoptively transferred MDSC or KIL cells

For some experiments, PMN-MDSC and M-MDSC isolated from splenocyte single cell suspensions using the Stemcell EasySep Mouse MDSC Isolation Kit per manufacturer recommendations and labelled with CellTracker Red CMTPX Dye (Thermo) per manufacturer recommendations prior to adoptive transfer. For other experiments, KIL were labelled with qTracker 585 (Thermo) per manufacturer recommendations prior to adoptive transfer. Tumors were digested into a single cell suspension as described and assessed by flow cytometry or images of whole tumor digests were acquired on an EVOS live cell imaging system (Thermo).

Murine and human immune cell sorting

Peripheral murine NK cells were isolated from splenic single cell suspensions using the mouse NK cell negative isolation kit on an AutoMACS Pro (Miltenyi) per manufacturer recommendations. Peripheral murine neutrophilic cells were isolated using the Ly6G Microbead positive selection kit (Miltenyi). Peripheral human NK cells were isolated using the human NK Cell Isolation Kit (Miltenyi) on PBMCs isolated from CPT collection tubes. Peripheral human myeloid cells were isolated using the CD15 or CD14 positive selection kits (Miltenyi) following an 80% Percoll gradient separation of whole blood collected in heparinized collection tubes. To isolate tumor infiltrating myeloid cells, murine or human tumors were digested into single cell suspensions as described and subjected to a 40/80% Percoll cell separation gradient. Murine neutrophilic cells were isolated from retrieved

leukocytes using a Ly6G positive selection kit, and human myeloid cells were isolated using CD15 or CD14 positive selection kits.

Real-time impedance analysis

MOC2 cells (5×10^3 cell/well) were plated in the presence or absence of DMSO control or SX-682. Other experiments were designed to measure MOC2 cytotoxicity when exposed to sorted NK or KIL cells. For detailed methods, see Supplementary Methods.

qPCR

Cells or whole tumor digests were lysed and RNA was purified using the RNEasy Mini Kit (Qiagen). cDNA was synthesized utilizing a high capacity reverse transcription kit with RNAse inhibitor (Applied Biosystems). A Taqman Universal PCR master mix was used to assess the relative expression of target genes compared to GAPDH on a Viia7 qPCR analyzer (Applied Biosystems). Primers were purchased from Thermo.

Human NK cell activation assay

Fresh sorted human healthy donor or HNSCC patient NK cells were stimulated with K562 cells at a K562-to-NK ratio of 1:1 with IFNα (1000 U/mL) as described (12). In some wells, fresh sorted healthy donor or HNSCC patient peripheral or tumor infiltrating CD15+ or CD14+ myeloid cells were added at different myeloid cell-to-NK ratios. In other wells, TGF-β mAb (clone 1D11.16.8, 2 μg/mL), catalase (300 μM), PD-L1 mAb (clone 29E.2A3, 2 μg/mL), L-NMMA (300 μM) or nor-NOHA (300 μM) were added. In co-incubation assays with specific inhibitors, MDSC were exposed to the inhibitors for one hour prior to co-incubation with NK cells, and the inhibitors remained in the well for the duration of the experiment. IFNγ production was measured via ELISpot assay (R&D Systems) per manufacturer recommendations and measured on an Immunospot ELISpot plate reader (Cellular Technology).

Statistics

Tests of significance between pairs of data are reported as p-values, derived using a student's t-test with a two-tailed distribution and calculated at 95% confidence. Comparison of multiple sets of data was achieved with analysis of variance (ANOVA) with Tukey's multiple comparisons. Survival analysis was determined by Log-Rank (Mantel-Cox) analysis. Error bars indicate standard deviation. Statistical significance was set to $p<0.05$. Analysis was performed using GraphPad Prism v7.

Results

To determine if tumor-bearing hosts developed dysfunctional NK cell immunity, splenic NK cells from wild-type mice bearing MOC2 tumors were studied. The fraction of NK within the splenocyte compartment was statistically decreased in tumor-bearing mice compared to naïve mice, as was the expression of the NK cell activating receptor NKG2D (Figure 1A), but these changes were of unclear biologic significance. Functional analysis of sorted NK cells from MOC2 tumor-bearing mice revealed decreased capacity to kill MOC2 target cells at a range of effector:target ratios compared to NK cells from naïve mice (Fig. 1B),

indicating suppressed function. This suppression of NK cell function appeared to be durable as incubation of NK cells for 24 hours prior to assessing their ability to kill MOC2 tumor cells did not restore the reduced ability of NK cells from MOC2 tumor-bearing mice to kill (Figure 1C). We next assessed peripheral myeloid cells. Both $Ly6G^{hi}Ly6C^{int}$ and $Ly6G^{low}LyC^{hi}$ myeloid splenocytes were significantly expanded in mice bearing MOC2 tumors compared to naïve mice ($p<0.001$, $p<0.01$, respectively, Fig. 1D). $Ly6G^{hi}Ly6C^{int}$ myeloid cells expressed high levels of CXCR2, $Ly6G^{low}LyC^{hi}$ myeloid cells expressed low CXCR2, and neither cell type expressed high levels of CXCR1. MOC2 tumors expressed the myeloid chemokines CXCL1/2/5 (Supplemental Fig. S1). To determine if these CXCR2 ligands correlated with myeloid cell chemotaxis, MOC tumors were assessed for myeloid cell infiltration. This analysis revealed that greater than 70% of all immune CD45.2+ cells within day 10 MOC2 tumors were myeloid lineage, with the vast majority displaying a $Ly6G^{hi}Ly6C^{int}$ phenotype (Fig. 1E). These $Ly6G^{hi}$ myeloid cells were sorted to high purity (Supplemental Fig. S2) and assessed for their ability to suppress NK cell function in real-time impedance assays. Tumor infiltrating $Ly6G^{hi}$ myeloid cells abrogated the ability of sorted NK cells from wild-type mice to kill MOC2 tumor targets, validating these cells as PMN-MDSC (Fig. 1F). Together these results demonstrated that mice bearing MOC2 tumors accumulated peripheral CXCR2+ PMN-MDSC that upon trafficking to tumor have the ability to suppress NK cell function.

Sorted NK cells are challenging as a study tool due to their low frequency in the peripheral blood and spleens of mice. KIL cells are a culturable murine NK cell line that can be expanded for *in vitro* and *in vivo* study(10,13). KIL cells killed MOC2 tumor targets to a greater degree at different effector:target ratios compared to sorted NK cells from wild-type mice (Fig. 2A). We next determined the ability of PMN-MDSC to suppress KIL function. Tumor PMN-MDSC abrogated the ability of KIL to kill MOC2 targets to a greater degree than peripheral PMN-MDSC (Fig. 2B), and tumor PMN-MDSC inhibited KIL killing capacity in a dose-dependent fashion (Fig. 2C). These results validated KIL as a tool to study the effects of murine MDSC on NK cells.

To study the mechanisms by which tumor PMN-MDSC suppressed KIL effector function, co-incubation experiments with neutralizing antibodies or specific inhibitors were performed. The addition of TGF-β mAb significantly abrogated the ability of tumor PMN-MDSC to suppress KIL killing of MOC2 cells (Fig. 3A). The addition of catalase, an inhibitor of extracellular hydrogen peroxide (H_2O_2), also reversed the ability of PMN-MDSC to suppress KIL effector function (Fig. 3B), although to a lesser degree than TGF-β mAb (Fig. 3C). The addition of PD-L1 mAb, the nitric oxide synthase (NOS) inhibitor L-NMMA or the arginase inhibitor nor-NOHA did not alter the ability of PMN-MDSC to suppress KIL effector function (Supplemental Fig. 3A–C). Given data that tumor PMN-MDSC suppressed kill function to a greater degree than peripheral PMN-MDSC, expression of cell surface TGF-β and superoxide dismutase 1 and 2 (SOD1/2) was measured in these subsets. Tumor PMN-MDSC expressed greater TGF-β and SOD1 compared to peripheral PMN-MDSC (Figure 3D&E). These data demonstrated that in the syngeneic MOC2 model, PMN-MDSC suppression of KIL effector function was mediated through TGF-β and H_2O_2.

Having established that immunosuppressive CXCR2+ PMN-MDSC infiltrate MOC2 tumors, we studied whether SX-682, an orally bio-available small molecule inhibitor of CXCR1/2, could alter PMN-MDSC trafficking and tumor accumulation. Mice bearing MOC2 tumors were treated with control chow or chow containing SX-682 for one week and assessed for PMN-MDSC accumulation by flow cytometry. SX-682 significantly decreased PMN-MDSC trafficking into MOC2 tumors (Fig.4A). SX-682 treatment of tumor-bearing mice did not alter the viability of tumor leukocytes (Figure 4B) and *ex vivo* exposure of sorted PMN-MDSC to SX-682 for 24 hours did not alter PMN-MDSC viability (Supplemental Fig. 4). Further, SX-682 treatment did not alter the proliferation of tumor PMN-MDSC in tumor bearing mice (Supplemental Fig. 5), suggesting that the primary mechanisms of SX-682 was inhibition of trafficking of PMN-MDSC into MOC2 tumors. To provide more definitive assessment of the ability of SX-682 to alter tumor trafficking of MDSC, fluorescently labelled MDSC were adoptively transferred into mice treated with control or SX-682 chow. SX-682 treatment abrogated the trafficking of adoptively transferred PMN-MSC and M-MDSC into MOC2 tumors (Figure 4C).

Inhibition of tumor PMN-MDSC accumulation alone with SX-682 did not alter tumor accumulation of endogenous NK cells, tumor-infiltrating NK cell activation status, or tumor infiltration of T-lymphocytes (Supplemental Fig. 6A–C). We next assessed if inhibiting PMN-MDSC tumor trafficking altered tumor accumulation of adoptively transferred KIL cells beyond that observed in control mice. Using fluorescently labelled KIL cells measured in whole tumor digests by fluorescent imaging and flow cytometry, pre-treatment of mice bearing MOC2 tumors with SX-682 significantly enhanced tumor accumulation of adoptive transferred KIL (Fig. 4D). Of note, KIL cells expressed CXCR1 but very low levels of CXCR2 (Figure 4E). Further, upon leukocyte isolation and stimulation, SX-682-treated tumor infiltrating NK lineage cells expressed IFNγ (Fig. 4F) and granzyme B (Fig. 4G) to a greater degree than control, which may correlate with increased killing capacity. Following *in vivo* SX-682 treatment, tumor PMN-MDSC expression of cell surface TGF-β or superoxide dismutase 1/2 genes, responsible for the generation of H_2O_2, was not significantly altered (Supplemental Fig. S7A&B). Similarly, the suppressive capacity of PMN-MDSC was not significantly altered following SX-682 treatment of tumor bearing mice or upon *ex vivo* exposure of sorted PMN-MDSC to SX-682 (Supplemental Fig. S7C&D). These results revealed that although SX-682 increased the tumor accumulation and activation status of adoptively transferred KIL cells primarily through inhibition of PMN-MDSC trafficking and not through direct alteration of PMN-MDSC function.

Based on these data, we next studied whether treatment of mice bearing established MOC2 tumors with SX-682 could enhance the therapeutic efficacy of adoptively transferred KIL cells. Treatment with SX-682 alone did not alter tumor progression (Fig. 5A). Adoptive transfer of KIL cells (5×10^6 cells/treatment for six treatments) delayed primary tumor growth in a subset of tumors and induced rejection of one of twenty (5%) tumors. Combination SX-682 treatment and KIL adoptive transfer consistently delayed primary tumor growth during the treatment period with significantly decreased tumor volume at day 21 compared to control or monotherapy groups (Fig.5B). Although the majority of MOC2 tumors rebounded following completion of treatment, combination SX-682 and KIL adoptive transfer led to significantly prolonged survival (Fig. 5C) and induced complete

tumor rejection in four of nineteen (21%) mice. Despite low expression of CXCR1/2, exposure to SX-682 *in vitro* did not significantly alter MOC2 tumor cell proliferation or cell cycle progression, viability, expression of NKG2D ligands or sensitivity to KIL killing (Supplemental Fig. 8A–F). Accepting murine KIL cells as a model of adoptively transferred cell therapy, these data demonstrated that partial abrogation of CXCR2+ myeloid cell trafficking into tumors with SX-682 enhanced the therapeutic efficacy of adoptively transferred NK cells. The mechanism appeared to be due to inhibition of PMN-MDSC trafficking alone, and not due to tumor cell-specific changes following SX-682 treatment.

The role of peripheral and tumor infiltrating myeloid cells in mediating T-lymphocyte immunosuppression within patients with HNSCC is well established(7,8). The role that both neutrophilic and monocytic myeloid cells may play in mediating NK cell immunosuppression in patients with HNSCC is less well understood. To clarify this role, we studied NK cells and myeloid cells from patients with newly diagnosed, advanced stage human papillomavirus-negative HNSCC. The NK cell fraction in circulation was not significantly different in patients with HNSCC compared to healthy donors (Fig. 6A). However, when stimulated with K562 cells in the presence of IFNα, NK cells from HNSCC patients were significantly less activated compared to NK from healthy donors, demonstrating reduced activation capacity (Fig. 6B). We next measured circulating putative MDSC based upon cell surface markers(14). Both HNSCC patients and healthy donors have high levels of circulating CD11b+CD33+CD15+CD14- total neutrophilic cells (Fig. 6C), but HNSCC patients have greater fraction of CD11b+CD33+CD15-CD14+HLA-DR^{low} monocytic cells compared to healthy donors (Fig. 6D). These CD14+HLA-DR^{low} cells have been shown to be MDSC, whereas CD14+HLA-DR^{hi} myeloid cells more likely represent macrophages(8). Although CD15+ cells expressed the greatest levels of CXCR1 and CXCR2, CD14+HLA-DR^{low} cells also expressed greater levels of these chemokine receptors compared to CD14+HLA-DRhi myeloid cells or other immune cells such as lymphocytes (Fig. 6E).

We next measured myeloid cell accumulation in freshly digested HNSCC tumors. Within HNSCCs, CD11b+CD33+ myeloid cells accounted for 38–55% of all viable CD45+ tumor leukocytes (Fig. 6F). Tumors accumulated greater numbers of CD15+ neutrophilic myeloid cells compared to CD14+HLA-DR^{low} monocytic myeloid cells (Fig. 6G). Tumors accumulated low numbers of NK cells (Fig. 6H). Sorted peripheral blood or tumor CD15+ or CD14+ myeloid cells were next assessed for their ability to suppress healthy donor NK cell activation. A validated IFNγ production assays (ELISpot) was chosen due to its reproducibility and low cell requirement. Although both suppressed NK cell activation, tumor infiltrating CD15+ and CD14+ myeloid cells displayed greater immunosuppressive capacity compared to peripheral CD15+ and CD14+ myeloid cells. Tumor infiltrating CD14+ myeloid cells suppressed NK cell activation to a greater degree than tumor infiltrating CD15+ myeloid cells. To study the mechanisms by which tumor infiltrating myeloid cells suppressed healthy donor NK effector function, co-incubation experiments with neutralizing antibodies or select inhibitors were performed (Fig. 6I). Similar to PMN-MDSC in mice, suppression of NK cells by CD15+ myeloid cells from HNSCC tumors was reversed in the presence of TGF-β mAb. Co-incubation with catalase to inhibit extracellular H_2O_2 had no obvious effect. Conversely, suppression of NK cells by CD14+ myeloid cells

from HNSCC tumors was reversed in the presence of the NOS inhibitor L-NMMA, but not other inhibitors. These data validated tumor infiltrating CD15+ and CD14+ myeloid cells as MDSC capable of suppressing NK cell function, and demonstrated the non-redundant mechanisms by which different subsets of tumor infiltrating MDSC can suppress effector cell function in patients with HNSCC. Cumulatively, these results support the inhibition of myeloid cell trafficking into tumors as a means of enhancing the therapeutic efficacy of adoptively transferred NK cells.

Discussion

This study provides evidence that inhibition of MDSC trafficking with a CXCR1/2 small molecule inhibitor can enhance the therapeutic efficacy of adoptively transferred NK cells. In the syngeneic oral cancer model MOC2, which harbors few genomic alterations and forms non-T cell inflamed tumors that are refractory to T cell-based immunotherapy(5,15,16), CXCR1/2 blockade with SX-682 decreased tumor infiltration of PMN-MDSC and increased tumor infiltration and activation of adoptively transferred murine NK cells. Mechanistically, PMN-MDSC abrogated murine NK cell function through production of TGF-β and H_2O_2. Arginase, NOS and PD-L1 did not appear to play dominant roles in NK suppression in this model. Additionally, SX-682 did not directly alter tumor cell proliferation, survival or sensitivity to NK killing and did not alter the suppressive capacity of the PMN-MDSC themselves. Together, these data support that the function and therapeutic efficacy of adoptively transferred NK cells can be enhanced primarily through the mechanism of reduced trafficking of immunosuppressive myeloid cells into the tumor microenvironment.

Our work validates previous reports demonstrating the ability of MDSC to suppress NK cell function, but adds translational relevance with the use of an orally bioavailable, clinical stage chemokine receptor inhibitor. Stiff et al. demonstrated nitric oxide-dependent suppression of NK cell-mediated antibody-dependent cell-mediated cytotoxicity (ADCC) by Gr-1+ myeloid cells in multiple murine cancer models(17). Although neutrophilic and monocytic myeloid cells cannot be differentiated with the Gr-1 marker, this work revealed globally that Gr-1+ MDSC can suppress another important NK cell function, ADCC, in addition to direct cytotoxicity. Our murine work revealed that NK cell direct cytotoxicity of tumor cells is inhibited through PMN-MDSC TGF-β and H_2O_2. Li et al. demonstrated the ability of total (Gr-1+) MDSC to suppress NK cell function through membrane-bound TGF-β, similar to our results(18). Additional work in monocytic MDSC isolated from patients with hepatocellular carcinoma revealed suppression of NK cell function through MDSC interaction with and blockade of NKp46, an activating co-receptor present on NK cells(19). MDSC suppress T cell function primarily through arginase, but this did not appear to be the case for suppression of NK cells(6,8). One interpretation of these data is that MDSC possess multiple mechanisms by which they can suppress the effector functions of NK cells. Inhibition of MDSC trafficking with a chemokine receptor inhibitor such as SX-682 to prevent their tumor infiltration altogether may be a more effective therapeutic strategy compared to attempts to block multiple, individual suppressive mechanisms.

SX-682 is an allosteric, small molecule inhibitor of CXCR1/2 currently undergoing clinical evaluation (NCT03161431). Previous work has demonstrated the ability of SX-682 to reduce tumor accumulation of CXCR2+ MDSC in mice to enhance the efficacy of T cell-based immunotherapy, including immune checkpoint blockade and adoptive T cell transfer(20,21). Our work is the first to demonstrate that a similar therapeutic strategy can be used to enhance the efficacy of adoptively transferred NK cells. Of note, SX-682 treatment did not enhance the accumulation or activation of endogenous NK cells. This suggests that approaches to increase the available pool of circulating effector immune cells such as adoptive cell transfer therapies may be needed in tumors that harbor intrinsic defects effector immune cell recruitment(5). Human NK cells express CXCR1, which brings up the possibility that SX-682 could abrogate trafficking of NK into tumors. However, KIL also express moderate levels of CXCR1, and tumor infiltration of adoptively transferred KIL was enhanced with SX-682 treatment, suggesting that CXCR1 expression alone is not sufficient to predict the ability of SX-682 to abrogate trafficking. This will need to be carefully studied in clinical trials.

Subclones of tumor cells within a heterogeneous tumor may acquire genomic alterations that disrupt IFN responses or antigen processing and presentation(1–3). These can confer resistance to T cell-based immunotherapy and represent a significant mechanism of treatment failure. NK cells kill tumor cell targets via antigen- and MHC-independent mechanisms. NK cell-based immunotherapy, such as adoptive transfer of *ex vivo* expanded clonal NK cells, may overcome these barriers and serve as an effective monotherapy or adjunct to T cell-based immunotherapy. Newly developed NK cell-based cellular therapies are currently under clinical study alone or in combination with other immune-oncology agents (NCT03027128, NCT03387111). This work provides the pre-clinical rationale for the combination of such NK cell therapies with a CXCR1/2 inhibitor designed to abrogate myeloid cell infiltration into the tumor microenvironment.

This work has also definitively demonstrated the presence of CXCR1/2+ neutrophilic and monocytic MDSC in the circulation of patients with HNSCC that traffic into the tumor microenvironment. The majority (>50%) of total tumor infiltrating immune cells were CD15+ or CD14+ MDSC, validated with functional data demonstrating suppression of NK activation by the sensitive ELISpot assay. Although others have demonstrated tumor infiltration of immunosuppressive CD14+HLA-DR^{low} monocytic MDSC(8) or the presence of CD14+ monocytic or CD66b+ neutrophilic MDSC in the peripheral blood of patients with HNSCC(7,22), our work is the first to assign different mechanisms of suppression based on neutrophilic or monocytic differentiation. In our dataset, tumor infiltrating MDSC were more suppressive than their circulating MDSC counterparts, and tumor infiltrating CD14+ M-MDSC demonstrated greater NOS-dependent immunosuppressive capacity compared to TGF-β-dependent suppression mediated by CD15+ PMN-MDSC on a cell-by-cell basis. Other reports characterizing the HNSCC tumor immune microenvironment have failed to consistently document high levels of circulating or tumor infiltrating neutrophilic cells(22–25), possibly due to the use of cryopreserved samples which can lead to the loss of neutrophilic cell populations(26,27).

Clear differences existed between murine and human MDSC that may be of translational importance. First, murine Ly6G^{hi} PMN-MDSC suppressed NK cell function through TGF-β and H_2O_2. Human CD15+ PMN-MDSC suppressed through TGF-β, but the H_2O_2 inhibitor catalase had no effect on suppressive capacity. Whether direct TGF-β inhibition alone would prove effective in reversing PMN-MDSC-mediated suppression of NK cell function requires further study. Human M-MDSC patently inhibited NK cell function through NOS function, but we were unable to comment on whether murine M-MDSC possess a similar mechanism due to the lack of accumulation of these cells in MOC2 tumors. Second, although murine PMN-MDSC expressed high levels of CXCR2 and low levels of CXCR1, both PMN-MDSC and M-MDSC in the circulation of HNSCC patients expressed greater levels of both CXCR1 and CXCR2 compared to other circulating immune cells. Whether dual inhibition of CXCR1 and CXCR2 with a small molecule inhibitor such as SX-682 inhibits tumor trafficking of MDSC to a greater degree than more specific CXCR2 inhibitors also requires further study.

A limitation of our study was how we isolated CD15+ and CD14+ myeloid cells from the peripheral blood and tumors of patients with HNSCC. Following Percoll gradients used to isolate total leukocytes from whole blood or tumor single cell digestions, positive magnetic selection was used to isolate total CD15+ or CD14+ populations. Subsets of myeloid cells certainly exist within each of these populations, including HLA-DR high or low CD14+ cells and high- or low-density CD15+ cells differentially expressing CD16, LOX-1 or fatty acid transport protein 2(28–30). Functional characterization of these individual cell subsets could yield important insights into MDSC biology in HNSCC, but in our experience, this type of isolation requires fluorescent activated cell sorting (FACS) that is traumatic to myeloid cells and disrupts their gene expression and viability. Conclusions from our work must be limited to whole CD15+ or CD14+ cell populations in the periphery or tumor microenvironment of patients with HNSCC.

In conclusion, we have established the importance of MDSC in mediating an NK cell-suppressive tumor microenvironment, and demonstrated that inhibition of PMN-MDSC trafficking with a dual CXCR1/2 small molecule inhibitor can enhance the therapeutic efficacy of adoptively transferred NK cells. NK cell-based cell therapies are under clinical study, and, similar to T cell-based immunotherapy strategies, combination with agents designed to enhance their efficacy through modulation of the tumor microenvironment will likely be required. NK cell-based immunotherapy may be particularly useful for patients with tumors that exclude T cells or harbor genomic alterations in IFN response or antigen processing and presentation genes. Human HNSCCs are heavily infiltrated with immunosuppressive PMN- and M-MDSC that possess multiple independent mechanisms of NK cell suppression. Cumulatively, these data support the clinical investigation of CXCR1/2 inhibition in combination with NK-cell-based immunotherapeutic strategies in patients with HNSCC.

Supplementary Material

Refer to Web version on PubMed Central for supplementary material.

Acknowledgements

The authors thank Dr. Christopher Silvin for assistance with flow cytometry, and Drs. James Hodge and Jason Redman for their critical review of this manuscript.

Financial support: S. Greene, Y. Robbins, W. Mydlarz, A. Huynh, N. Schmitt, J. Friedman, P. Clavijo and C. Allen were supported by the Intramural Research Program of the NIH, National Institute on Deafness and Other Communication Disorders, project number ZIA-DC000087. S. Greene was supported through the NIH Medical Research Scholars Program, a public-private partnership supported jointly by the NIH and contributions to the Foundation for the NIH from the Doris Duke Charitable Foundation (DDCF Grant #2014194), the American Association for Dental Research, the Colgate-Palmolive Company, Genentech, Elsevier, and other private donors.

References

1. Zaretsky JM, Garcia-Diaz A, Shin DS, Escuin-Ordinas H, Hugo W, Hu-Lieskovan S, et al. Mutations Associated with Acquired Resistance to PD-1 Blockade in Melanoma. N Engl J Med 2016;375(9):819–29. [PubMed: 27433843]
2. Sade-Feldman M, Jiao YJ, Chen JH, Rooney MS, Barzily-Rokni M, Eliane JP, et al. Resistance to checkpoint blockade therapy through inactivation of antigen presentation. Nat Commun 2017;8(1):1136. [PubMed: 29070816]
3. McGranahan N, Rosenthal R, Hiley CT, Rowan AJ, Watkins TBK, Wilson GA, et al. Allele-Specific HLA Loss and Immune Escape in Lung Cancer Evolution. Cell 2017;171(6):1259–71. [PubMed: 29107330]
4. Davis RJ, Van Waes C, Allen CT. Overcoming barriers to effective immunotherapy: MDSCs, TAMs, and Tregs as mediators of the immunosuppressive microenvironment in head and neck cancer. Oral Oncol 2016;58:59–70. [PubMed: 27215705]
5. Clavijo PE, Moore EC, Chen J, Davis RJ, Friedman J, Kim Y, et al. Resistance to CTLA-4 checkpoint inhibition reversed through selective elimination of granulocytic myeloid cells. Oncotarget 2017;8(34):55804–20. [PubMed: 28915554]
6. Davis RJ, Moore EC, Clavijo PE, Friedman J, Cash H, Chen Z, et al. Anti-PD-L1 Efficacy Can Be Enhanced by Inhibition of Myeloid-Derived Suppressor Cells with a Selective Inhibitor of PI3Kdelta/gamma. Cancer Res 2017;77(10):2607–19. [PubMed: 28364000]
7. Lang S, Bruderek K, Kaspar C, Hoing B, Kanaan O, Dominas N, et al. Clinical Relevance and Suppressive Capacity of Human Myeloid-Derived Suppressor Cell Subsets. Clin Cancer Res 2018;24(19):4834–44. [PubMed: 29914893]
8. Vasquez-Dunddel D, Pan F, Zeng Q, Gorbounov M, Albesiano E, Fu J, et al. STAT3 regulates arginase-I in myeloid-derived suppressor cells from cancer patients. J Clin Invest 2013;123(4):1580–9. [PubMed: 23454751]
9. Judd NP, Winkler AE, Murillo-Sauca O, Brotman JJ, Law JH, Lewis JS Jr., et al. ERK1/2 regulation of CD44 modulates oral cancer aggressiveness. Cancer Res 2012;72(1):365–74. [PubMed: 22086849]
10. Friedman J, Morisada M, Sun L, Moore EC, Padget M, Hodge JW, et al. Inhibition of WEE1 kinase and cell cycle checkpoint activation sensitizes head and neck cancers to natural killer cell therapies. J Immunother Cancer 2018;6(1):59. [PubMed: 29925431]
11. Davis RJ, Silvin C, Allen CT. Avoiding phagocytosis-related artifact in myeloid derived suppressor cell T-lymphocyte suppression assays. J Immunol Methods 2017;440:12–8. [PubMed: 27856191]
12. Lion E, Smits EL, Berneman ZN, Van Tendeloo VF. Quantification of IFN-gamma produced by human purified NK cells following tumor cell stimulation: comparison of three IFN-gamma assays. J Immunol Methods 2009;350(1–2):89–96. [PubMed: 19733573]
13. DeHart SL, Heikens MJ, Tsai S. Jagged2 promotes the development of natural killer cells and the establishment of functional natural killer cell lines. Blood 2005;105(9):3521–7. [PubMed: 15650053]
14. Bronte V, Brandau S, Chen SH, Colombo MP, Frey AB, Greten TF, et al. Recommendations for myeloid-derived suppressor cell nomenclature and characterization standards. Nat Commun 2016;7:12150. [PubMed: 27381735]

15. Onken MD, Winkler AE, Kanchi KL, Chalivendra V, Law JH, Rickert CG, et al. A surprising cross-species conservation in the genomic landscape of mouse and human oral cancer identifies a transcriptional signature predicting metastatic disease. Clin Cancer Res 2014;20(11):2873–84. [PubMed: 24668645]
16. Moore E, Clavijo PE, Davis R, Cash H, Van Waes C, Kim Y, et al. Established T Cell-Inflamed Tumors Rejected after Adaptive Resistance Was Reversed by Combination STING Activation and PD-1 Pathway Blockade. Cancer Immunol Res 2016;4(12):1061–71. [PubMed: 27821498]
17. Stiff A, Trikha P, Mundy-Bosse B, McMichael E, Mace TA, Benner B, et al. Nitric Oxide Production by Myeloid-Derived Suppressor Cells Plays a Role in Impairing Fc Receptor-Mediated Natural Killer Cell Function. Clin Cancer Res 2018;24(8):1891–904. [PubMed: 29363526]
18. Li H, Han Y, Guo Q, Zhang M, Cao X. Cancer-expanded myeloid-derived suppressor cells induce anergy of NK cells through membrane-bound TGF-beta 1. J Immunol 2009;182(1):240–9. [PubMed: 19109155]
19. Hoechst B, Voigtlaender T, Ormandy L, Gamrekelashvili J, Zhao F, Wedemeyer H, et al. Myeloid derived suppressor cells inhibit natural killer cells in patients with hepatocellular carcinoma via the NKp30 receptor. Hepatology 2009;50(3):799–807. [PubMed: 19551844]
20. Sun L, Clavijo PE, Robbins Y, Patel P, Friedman J, Greene S, et al. Inhibiting myeloid-derived suppressor cell trafficking enhances T cell immunotherapy. JCI Insight 2019;4(7).
21. Lu X, Horner JW, Paul E, Shang X, Troncoso P, Deng P, et al. Effective combinatorial immunotherapy for castration-resistant prostate cancer. Nature 2017;543(7647):728–32. [PubMed: 28321130]
22. Chikamatsu K, Sakakura K, Toyoda M, Takahashi K, Yamamoto T, Masuyama K. Immunosuppressive activity of CD14+ HLA-DR- cells in squamous cell carcinoma of the head and neck. Cancer Sci 2012;103(6):976–83. [PubMed: 22360618]
23. Chen WC, Lai CH, Chuang HC, Lin PY, Chen MF. Inflammation-induced myeloid-derived suppressor cells associated with squamous cell carcinoma of the head and neck. Head Neck 2017;39(2):347–55. [PubMed: 27696591]
24. Tsai MS, Chen WC, Lu CH, Chen MF. The prognosis of head and neck squamous cell carcinoma related to immunosuppressive tumor microenvironment regulated by IL-6 signaling. Oral Oncol 2019;91:47–55. [PubMed: 30926062]
25. Sampath S, Won H, Massarelli E, Li M, Frankel P, Vora N, et al. Combined modality radiation therapy promotes tolerogenic myeloid cell populations and STAT3-related gene expression in head and neck cancer patients. Oncotarget 2018;9(13):11279–90. [PubMed: 29541413]
26. Kuhns DB, Long Priel DA, Chu J, Zarember KA. Isolation and Functional Analysis of Human Neutrophils. Curr Protoc Immunol 2015;111:7. [PubMed: 26528633]
27. Trellakis S, Bruderek K, Hutte J, Elian M, Hoffmann TK, Lang S, et al. Granulocytic myeloid-derived suppressor cells are cryosensitive and their frequency does not correlate with serum concentrations of colony-stimulating factors in head and neck cancer. Innate Immun 2013;19(3):328–36. [PubMed: 23160385]
28. Brandau S, Trellakis S, Bruderek K, Schmaltz D, Steller G, Elian M, et al. Myeloid-derived suppressor cells in the peripheral blood of cancer patients contain a subset of immature neutrophils with impaired migratory properties. J Leukoc Biol 2011;89(2):311–7. [PubMed: 21106641]
29. Condamine T, Dominguez GA, Youn JI, Kossenkov AV, Mony S, Alicea-Torres K, et al. Lectin-type oxidized LDL receptor-1 distinguishes population of human polymorphonuclear myeloid-derived suppressor cells in cancer patients. Sci Immunol 2016;1(2).
30. Veglia F, Tyurin VA, Blasi M, De Leo A, Kossenkov AV, Donthireddy L, et al. Fatty acid transport protein 2 reprograms neutrophils in cancer. Nature 2019;569(7754):73–8. [PubMed: 30996346]

Translational relevance

Tumors can escape T cell immunity through genomic alterations in interferon and antigen presentation pathway genes. Such tumors may be amenable to NK cell-based immunotherapy, but similar to T cell-based immunotherapy, treatment efficacy may be limited by an immunosuppressive tumor microenvironment. Here, we demonstrated that SX-682, a small molecule inhibitor of the myeloid chemokine receptors CXCR1 and CXCR2, abrogated tumor trafficking of myeloid derived suppressor cells and enhanced the tumor infiltration, activation, and therapeutic efficacy of adoptively transferred NK cells. Along with validation of the role that myeloid derived suppressor cells play in mediating an immunosuppressive microenvironment in HNSCC patients, these data support the clinical study of NK cell immunotherapy in combination with CXCR1/2 inhibition targeting myeloid cells, particularly in patients harboring non-T cell inflamed tumors.

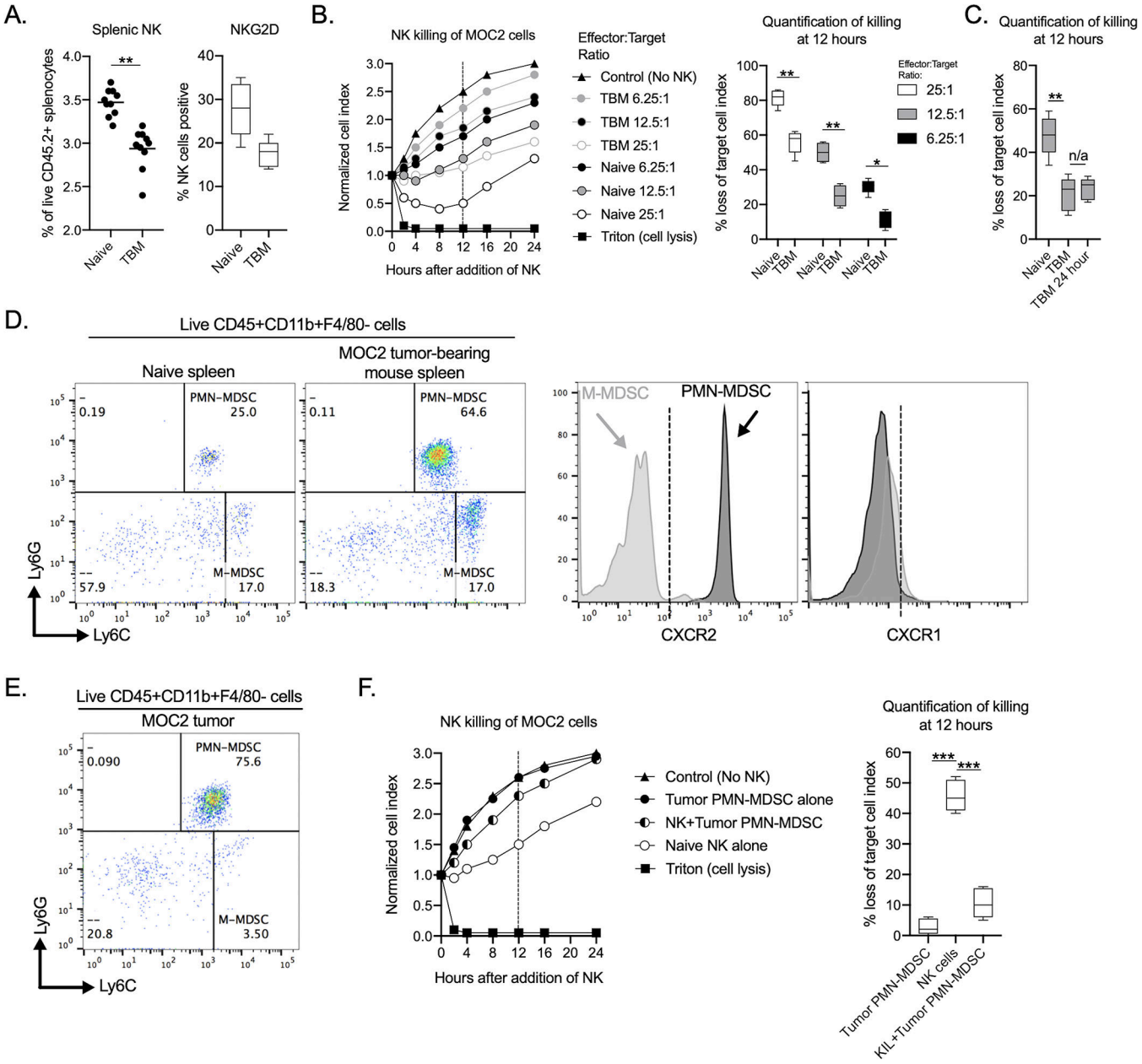

Figure 1. MOC2 tumor bearing mice accumulated PMN-MDSC and dysfunctional NK cells

Spleens from non-tumor bearing (naïve) or day 10 MOC2 tumor bearing wild-type B6 mice (TBM) were assessed for NK cell accumulation (**A**) or NKG2D cell surface expression (**B**) by flow cytometry (n=10). **B**, Splenic NK cells from naïve or day 10 MOC2 tumor bearing mice were isolated via magnetic selection and assessed for their ability to kill MOC2 tumors cells at different E:T ratios via impedance analysis. Representative impedance plot shown on the left, with quantification of NK killing of MOC2 cells at 12 hours on the right. **C**, NK cells were isolated as in B, incubated for 24 hours, and quantification of MOC2 killing by impedance analysis was performed with quantification at 12 hours shown. **D**, Spleens from naïve and day 10 MOC2 tumor bearing mice were assessed for myeloid cells by flow cytometry. Representative dot plots of live, $CD45.2^{+}CD11b^{+}F4/80^{-}$ myeloid cells are shown

(frequencies shown represent frequencies of this myeloid cell gate). PMN-MDSC were defined as $Ly6G^{hi}Ly6C^{int}$ and M-MDSC as $Ly6G^{low}Ly6C^{hi}$. To the right are representative histograms of chemokine receptor expression on MDSC subsets. **E**, Representative dot plot of live, $CD45.2^{+}CD11b^{+}F4/80^{-}$ myeloid cells from a day 10 MOC2 tumor. **F**, PMN-MDSC (PMN-MDSC-to-NK ratio of 3:1) isolated from MOC2 tumors were assessed for their ability to suppress the ability of isolated splenic NK cells to kill MOC2 tumor cells (NK-to-MOC2 ratio of 10:1) via impedance analysis. Representative impedance plot shown on the left, with quantification of NK killing of MOC2 cells at 12 hours on the right (n=5). All representative data shown from one of at least three independent experiments with similar results. *, p<0.05; **, p<0.01; ***, p<0.001

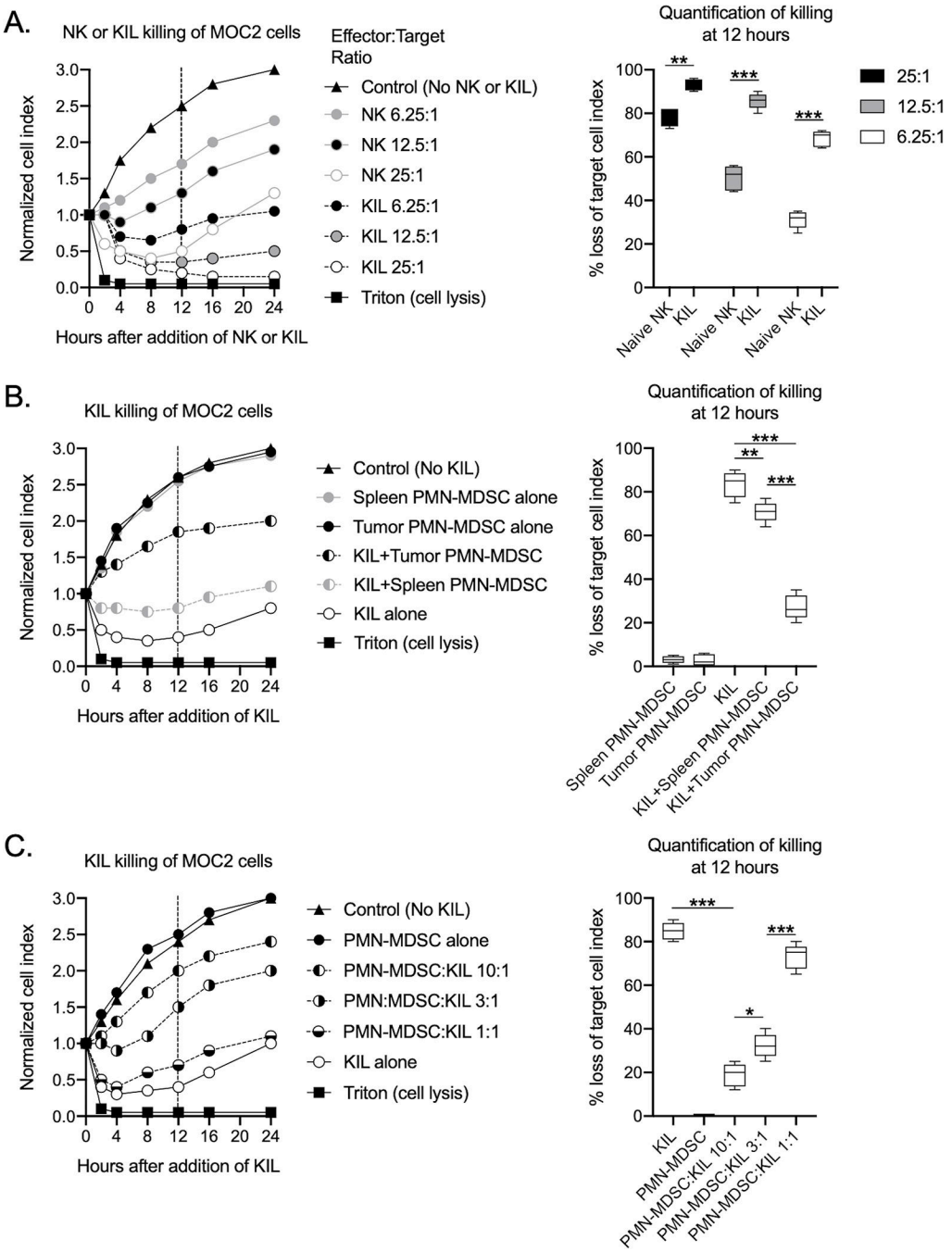

Figure 2. Tumor PMN-MDSC suppressed the effector function of KIL cells

A, Isolated splenic NK cells and KIL were assessed for their ability to kill MOC2 tumors cells at different E:T ratios via impedance analysis. Representative impedance plot on the left, with quantification of NK killing of MOC2 cells at 12 hours on the right. **B**, KIL were assessed for their ability to kill MOC2 tumors cells (NK-to-MOC2 ratio of 10:1) in the presence of isolated splenic or tumor PMN-MDSC at a PMN-MDSC-to-KIL ration of 3:1 via impedance analysis. Representative impedance plot on the left, with quantification of NK killing of MOC2 cells with or without PMN-MDSC at 12 hours on the right. **C**, PMN-

MDSC isolated from MOC2 tumors were assessed for their ability to inhibit KIL killing of MOC2 tumor cells (NK-to-MOC2 ratio of 10:1) over a range of PMN-MDSC-to-KIL ratios. Representative impedance plot on the left, with quantification of NK killing of MOC2 cells with or without PMN-MDSC at 12 hours on the right. All representative data shown from one of at least three independent experiments with similar results. *, $p<0.05$; **, $p<0.01$; ***, $p<0.001$

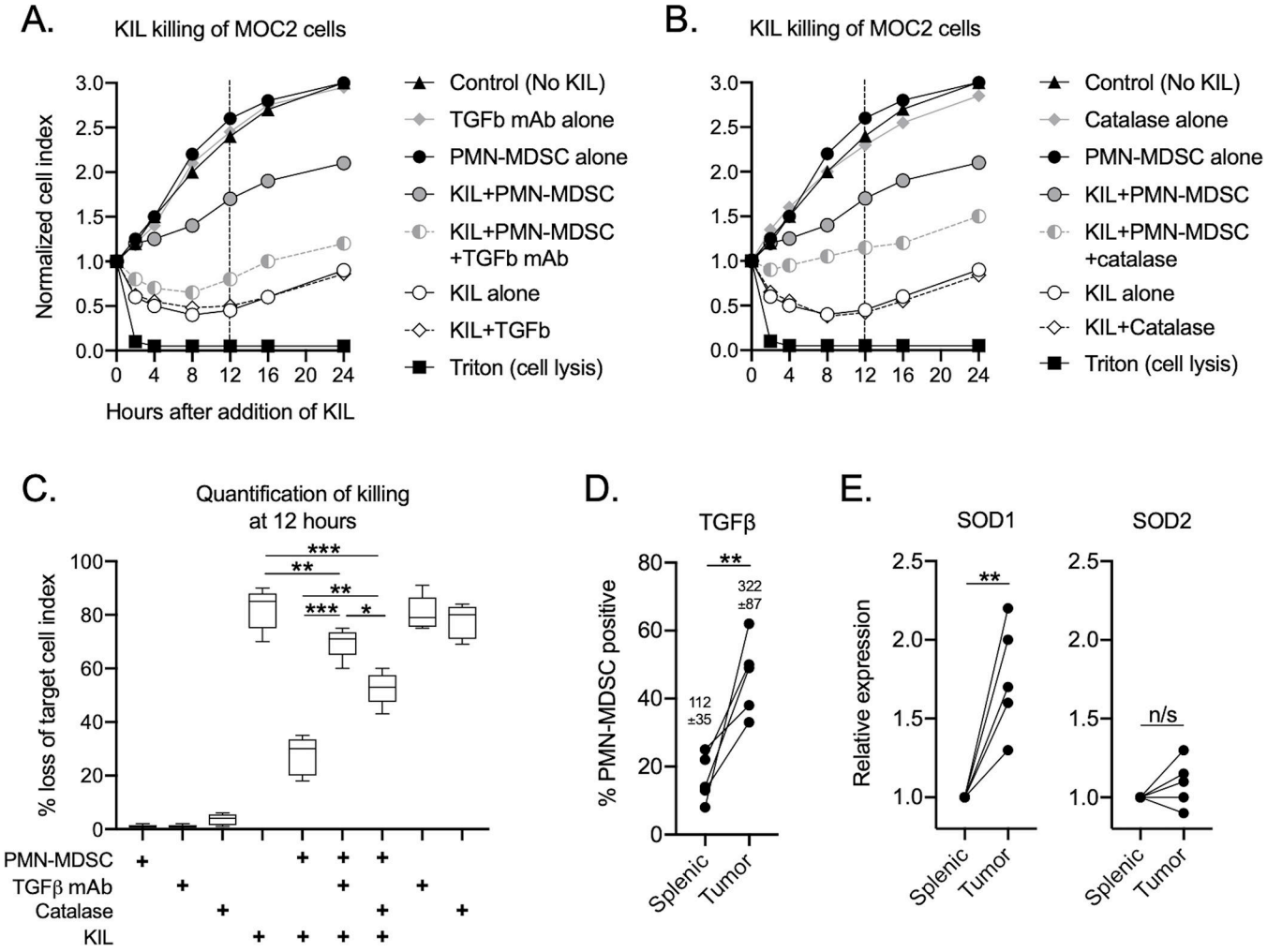

Figure 3. Tumor PMN-MDSC inhibited KIL effector function through TGFβ and H_2O_2

PMN-MDSC isolated from MOC2 tumors (PMN-MDSC-to-NK ratio of 3:1) were assessed for their ability to inhibit KIL killing of MOC2 tumor cells (NK-to-MOC2 ratio of 10:1) in the presence or absence of TGFβ neutralizing antibody (**A**) or the H_2O_2 inhibitor catalase (**B**). Representative impedance plots shown. **C**, quantification of NK killing of MOC2 cells with or without PMN-MDSC and inhibitors at 12 hours. Quantification of cell surface TGFβ expression by flow cytometry (**D**) or SOD1/2 expression by qPCR (**E**) was determined for splenic or tumor infiltrating PMN-MDSC. All representative data shown from one of two independent experiments with similar results. **, $p<0.01$; ***, $p<0.001$

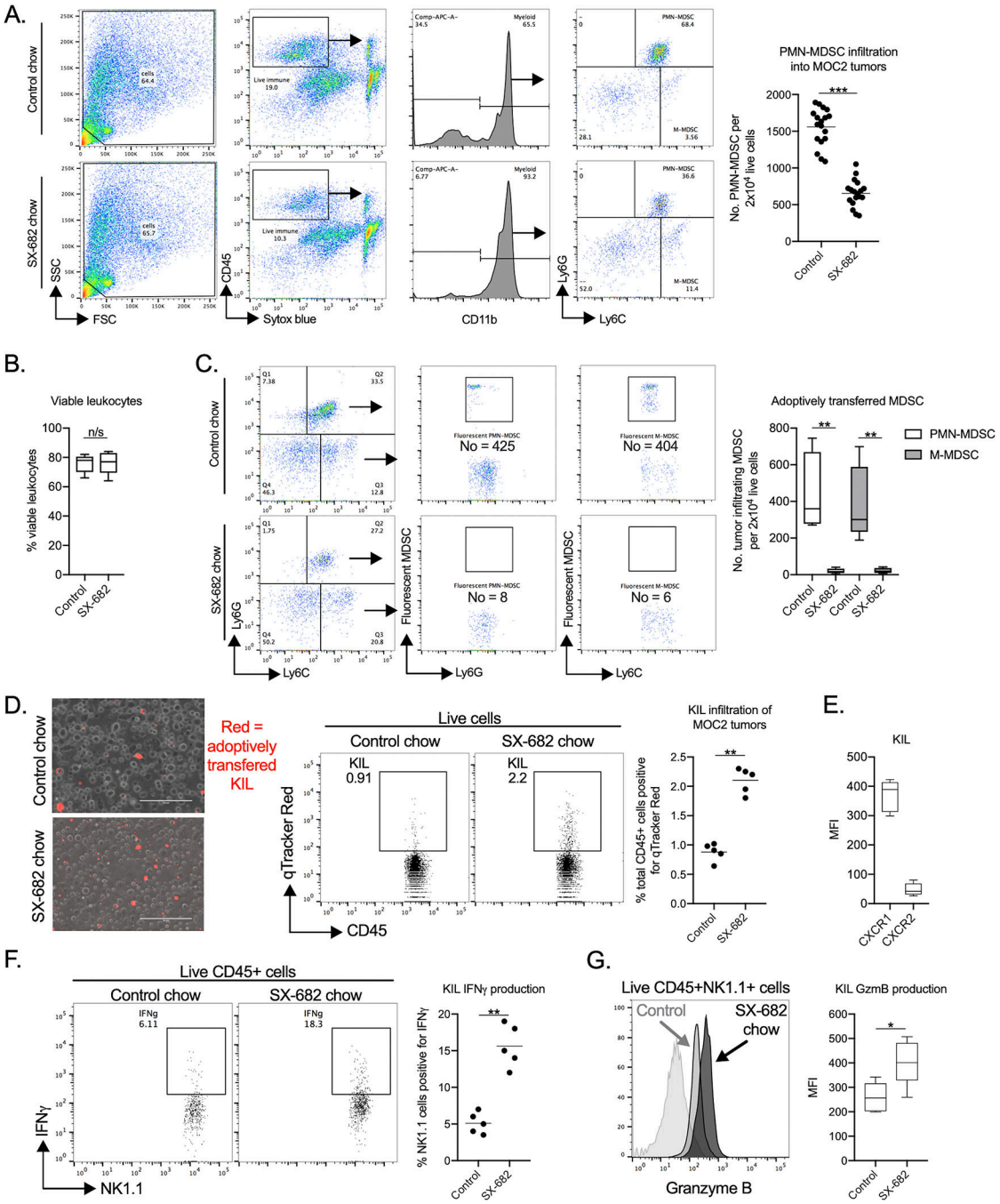

Figure 4. SX-682 inhibited PMN-MDSC trafficking and enhanced tumor infiltration and activation of adoptively transferred KIL

A, MOC2 tumor bearing mice were treated with SX-682 starting at day 7. At day 14, tumor single cell suspensions were assessed for live, $CD45.2^{+}CD11b^{+}F4/80^{-}$ myeloid cells by flow cytometry. Representative dot plots of gating strategy shown on the left, quantification (n=18) shown on the right. **B**, viability of CD45.2+ tumor leukocytes was determined by flow cytometry, quantification (n=18) shown. **C**, splenic PMN-MDSC or M-MDSC isolated from day mice bearing 14 day-old MOC2 tumors were fluorescently labelled and adoptively

transferred (1×10^7 MDSC/mouse, n=5) into mice bearing 15 day-old MOC2 tumors treated with control or SX-682 chow beginning on day 7. Tumors were harvested and analyzed by flow cytometry 18 hours after adoptive transfer. Representative dot plots shown on the left, quantification of the number of fluorescently labelled MDSC that trafficked into tumors shown on the right. **D**, KIL were fluorescently labelled and adoptively transferred into day 10 MOC2 tumors in mice treated with or without SX-682 beginning at day 7. Four hours after injection of KIL, tumor single cell suspensions were assessed for KIL infiltration via fluorescent imaging (left panels) or flow cytometry. Representative dot plots are shown, with quantification (n=5) shown on the right. KIL were adoptively transferred into day 10 MOC2 tumors in mice treated with or without SX-682 beginning at day 7. **E**, CXCR1 and CXCR2 expression on KIL cells was assessed by flow cytometry, quantification shown. Twenty-four hours after injection, enriched leukocytes obtained via density gradient from MOC2 tumor single cell suspensions were assessed for IFN**γ** (**F**) or granzyme B (**G**) positivity following stimulation (PMA/Iono with brefeldin) by flow cytometry. Representative dot plots or histograms are shown on the left, with quantification (n=5) shown on the right. All representative data shown from one of at least two independent experiments with similar results. *, p<0.05; **, p<0.01; ***, p<0.001

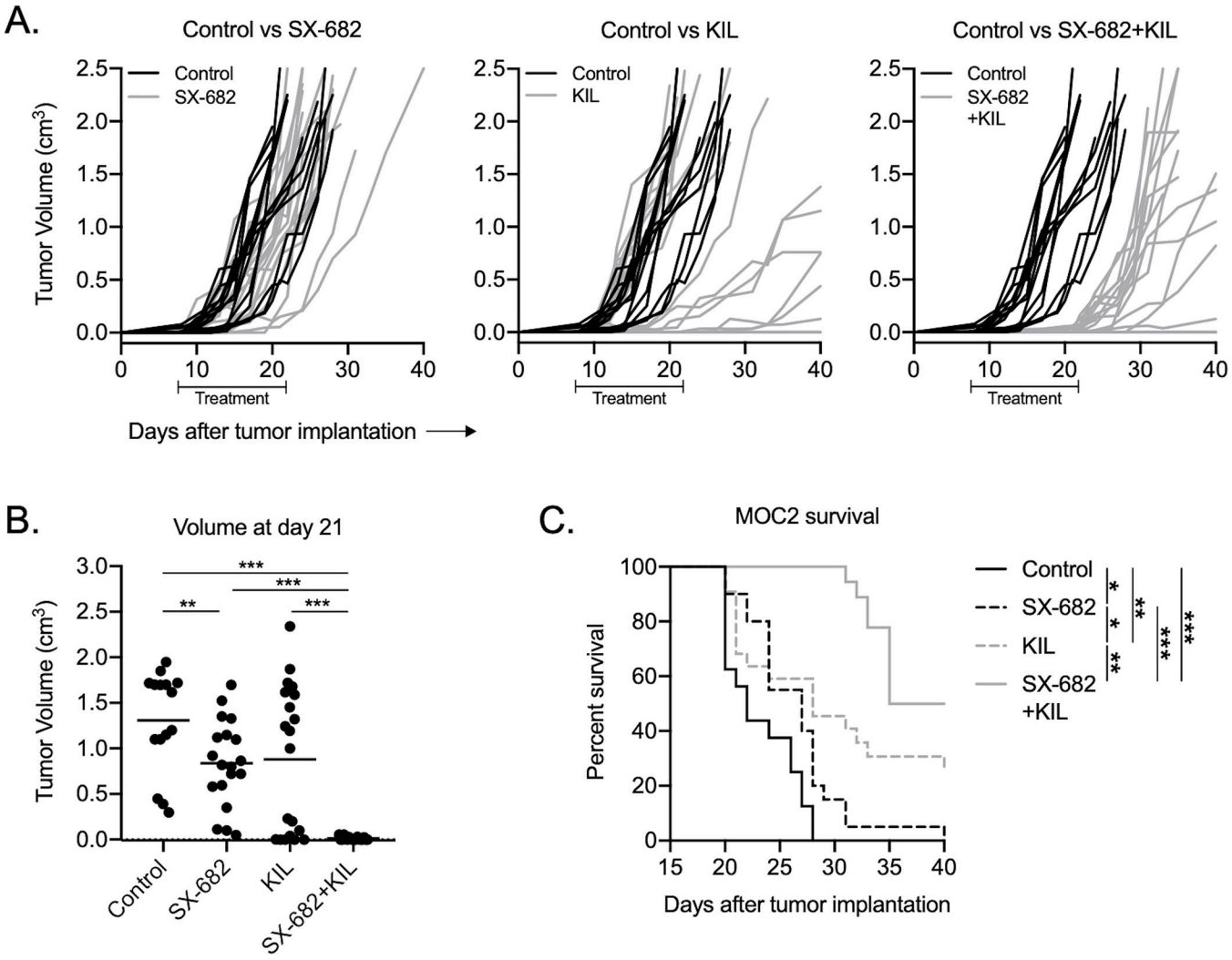

Figure 5. Inhibition of PMN-MDSC trafficking enhanced the efficacy of adoptively transferred KIL in mice bearing MOC2 tumors

A, Wild-type C57BL/6 mice harboring MOC2 tumors were treated with SX-682 (starting day 7, treatment for 7 days) alone or in combination with adoptively transferred KIL (starting day 7, 5×10^6 cells three times weekly for 2 weeks) and assessed for primary tumor growth (n=18–20 mice/group). Each line represents individual tumor growth. **B**, Day 20 tumor volumes for each treatment condition. **C**, Survival of treated MOC tumor-bearing mice, Kaplan-Meier survival curve shown. Cumulative data from three independent experiments shown. *, p<0.05; **, p<0.01; ***, p<0.001

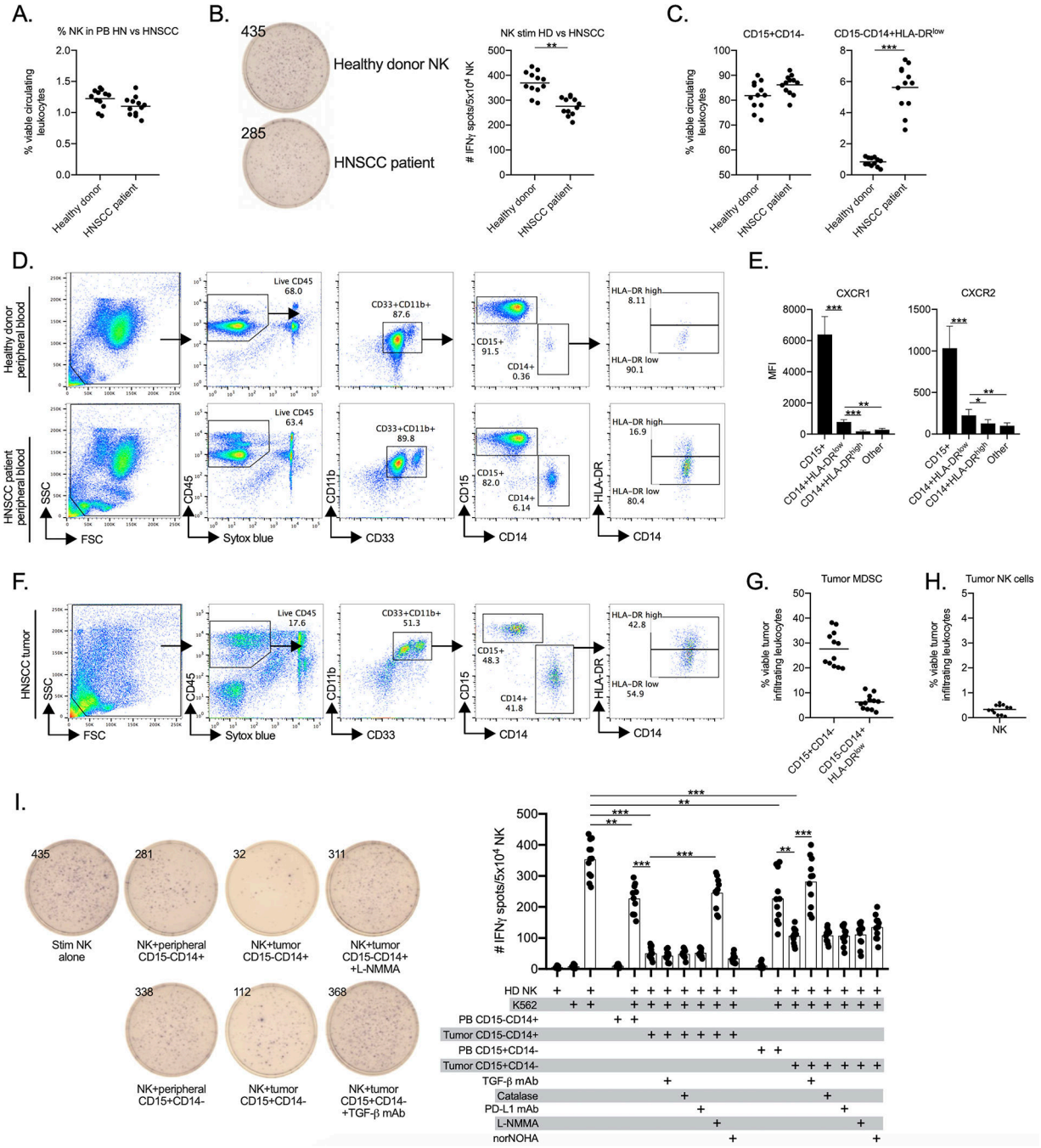

Figure 6. HNSCC patient peripheral blood and tumors harbor CD15+ and CD14+ MDSC that suppress NK cells through multiple mechanisms

A, peripheral blood from patients with advanced HNSCC or healthy donors (n=12) was assessed for circulating NK cells by flow cytometry. **B**, sorted peripheral NK from HNSCC patients or healthy donors (n=12) were stimulated and assessed for IFNγ production by ELISpot. Representative ELISpot well photomicrographs are shown on the left (spot counts inset), with absolute spot counts shown on the right. Peripheral blood from patients with advanced HNSCC or healthy donors (n=12) was assessed for circulating NK cells by flow

cytometry. Peripheral blood CD15+CD14- and CD15-CD14HLA-DR^{low} myeloid cells are quantified in **C**. Gating strategy and representative dot plots are shown in **D**. **E**, MFI of CXCR1 and CXCR2 expression on HNSCC patient peripheral blood (n=10) myeloid cells and NK cells. Other cells indicates B and T lymphocytes. **F**, HNSCC tumor single cell suspensions were assessed for infiltration of myeloid cells by flow cytometry. Gating strategy and representative dot plots is shown. **G**, quantification (n=12) of CD15+CD14- and CD15-CD14+HLA-DR^{low} cells. **H**, tumor infiltration of live, CD45+CD56+CD3- NK cells was assessed by flow cytometry, quantification (n=12) is shown. **I**, sorted health donor NK cells were stimulated in the presence or absence of sorted CD15+CD14- or CD15-CD14+ peripheral blood or tumor infiltrating myeloid cells and assessed for IFNγ production via ELISpot assay (n=10–12). Functional inhibitors of TGF-β (TGF-β mAb), H_2O_2 (catalase), PD-L1 (PD-L1 mAb), NOS (L-NMMA) or arginase (norNOHA) were used in some wells. Representative ELISpot well photomicrographs are shown on the left (dot counts inset), absolute spot counts shown on the right.

**, p<0.01; ***, p<0.001